ACS APPLIED MATERIALS & INTERFACES

Research Article

www.acsami.org

Maximizing the Relaxivity of Gd-Complex by Synergistic Effect of HSA and Carboxylfullerene

Mingming Zhen,[†,‡] Junpeng Zheng,[†,‡] Lei Ye,[†,‡] Shumu Li,[†,‡] Chan Jin,[∥] Kai Li,[§] Dong Qiu,[†] Hongbin Han,[§] Chunying Shu,*[,†] Yongji Yang,[∥] and Chunru Wang*[,†]

[†]Beijing National Laboratory for Molecular Sciences, Key Laboratory of Molecular Nanostructure and Nanotechnology, Institute of Chemistry, Chinese Academy of Sciences, Beijing 100190, China

[‡]Graduate School of Chinese Academy of Sciences, Beijing 100049, China

[§]Department of Radiology, Peking University Third Hospital, Beijing 100083, China

[∥]Institute of Biophysics, Second Military Medical University, Shanghai 200433, China

S *Supporting Information*

ABSTRACT: Macromolecular magnetic resonance imaging (MRI) contrast agent Gd-DTPA-HSA (DTPA, diethylene triamine pentacetate acid; HSA, human serum albumin) as a model has been successfully conjugated with trimalonic acid modified C_{60} for contrast enhancement at clinically used magnetic field strength. The Gd-DTPA-HSA-C_{60} conjugate exhibit maximal relaxivity (r_1 = 86 mM^{-1} s^{-1} at 0.5 T, 300 K) reported so far, which is much superior to that of the control Gd-DTPA-HSA (r_1 = 38 mM^{-1} s^{-1}) under the same condition and comparable to the theoretical maximum (r_1 = 80−120 mM^{-1} s^{-1}, at 20 MHz and 298 K), indicating the synergistic effect of HSA and carboxylfullerene on the increased contrast enhancement. TEM characterization reveals that both Gd-DTPA-HSA-C_{60} and Gd-DTPA-HSA can penetrate the cells via endocytosis and transmembrane, respectively, suggesting the potential to sensitively image the events at the cellular and subcellular levels. In addition, the fusion of fullerene with Gd-DTPA-HSA will further endow the resulting complex with photodynamic therapy (PDT) property and thus combine the modalities of therapy (PDT) and diagnostic imaging (MRI) into one entity. More importantly, the payloaded Gd-DTPA may substitute for other more stable Gd-DOTA and HSA as a theranostic package can further work as a drug delivery carrier and effectively control drug release through proteolysis.

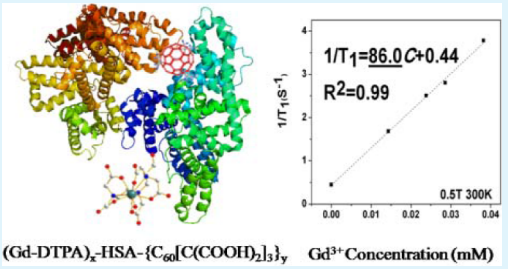

KEYWORDS: *macromolecular MRI contrast agents, contrast enhancement, carboxylfullerene, theranostics, photosensitizer, intracellular imaging*

INTRODUCTION

Molecular magnetic resonance imaging (MRI) emerging as a noninvasive and nonradiative technique with superb spatial and temporal resolution offers the potential to visualize molecular events related with diseases and abnormalities at the cellular and subcellular level.[1−6] To increase the sensitivity of the interested pathological processes and diagnostic confidence, researchers frequently administer paramagnetic substances as contrast agents (CAs) to increase the contrast between normal tissues and pathological tissues and delineate the boundary of tumor clearly for surgery.[7−9] Currently used MRI contrast agents are mainly small molecular gadolinium poly(amino carboxylate) chelates since the first approval of $[Gd(DTPA)(H_2O)]^{2-}$ in 1987 by FDA. However, there are still many deficiencies for the small molecular MRI CAs like Gd-DTPA, such as extracellular distribution, low sensitivity, and nonspecificity. According to the classic relaxivity theory, the Solomon−Bloembergen−Morgan (SBM) theory, great effort has been addressed to the modification of ligands to optimize the pivotal parameters that determine the relaxivity,[10−13] such as the hydration number of water molecules (q) in the coordination shell, the exchange rate of the coordinated water with the bulk water,[14,15] the rotational correlation time, τ_R[16−18] and so on. Up to date, lots of work has been carried out on Gd-based macromolecular MRI CAs by field-cycling MRI scanners since the relaxivities of obtained macromolecular MRI CAs are usually field strength dependent,[19] much different from those of small molecular MRI contrast agents,[20,21] and the results usually display a maximal relaxivity at low fields (20−40 MHz),[22,23] which may ascribe to the proximity of the proton Larmor frequency at the applied magnetic field strength.

To increase τ_R, one effective strategy is to attach the ligand with macromolecules, leading to corresponding increase of relaxivities.[15,16,24−26] HSA as one of the most used macromolecular carriers in biomedicine has been successfully conjugated with Gd-DTPA[27] or MS-325 to enhance the blood pool contrast, as it is biocompatible, easily multifunctional, and competent for a carrier of drug delivery.[28] For

Received: May 10, 2012
Accepted: June 18, 2012
Published: June 18, 2012

   dx.doi.org/10.1021/am300817z | ACS Appl. Mater. Interfaces 2012, 4, 3724−3729

example, albumin-Gd-DTPA with larger molecular weight and longer blood retention times has been used as blood pool MRI contrast agent.[29] MS-325 (Vasovist/AngioMARK, Bayer HealthCare, Mallinckrodt) itself as small molecular MRI contrast agent can slightly improve the blood pool MRI contrast via intermolecular interaction with protein.[19] However, the efficacy of Gd-complex to relax water proton is still far from the predicted by theory.

In recent years, great interest has been addressed on carbon-based nanomaterials such as fullerenes for biological applications (photodynamic therapy, drug delivery) because of their unique physical, chemical, and biological properties.[30−35] Photodynamic therapy (PDT) has emerged as an important technique in cancer treatment since it is less invasive, leaving the surrounding healthy tissues and cells undamaged. Fullerene (C_{60}) with a long-lived triplet excited state can produce $^1O_2$ by energy transfer with extremely high quantum yield (Φ_Δ = 0.96, λ_{exc} = 532 nm) and therefore exhibit superior photosensitization performance in comparison with commonly used porphyrins. The HSA-fullerene conjugate has been reported and studied for its photodynamic property.[36,37] Herein, we used Gd-DTPA-HSA as a useful precursor to conjugate with carboxylfullerene to further enhance the contrast at clinically used magnetic field strength. The resulting macromolecular complex, Gd-DTPA-HSA-C_{60}, therefore successfully combines highly efficient diagnostic imaging (MRI) and PDT property into one entity.

MATERIALS AND METHODS

Material. All chemicals, unless otherwise stated, were purchased from commercial sources and used without further purification. HSA was bought from XinJingKe Biotechnology Co., Ltd. Beijing; DTPA anhydride, $GdCl_3{\cdot}6H_2O$, EDC and NHS (EDC, 1-Ethyl-3-(3-dimethylaminopropyl) Carbodiimide Hydrochloide; NHS, N-Hydroxysulfosuccinimide) were purchased from Alfa Aesar. The culture media DMEM (Hyclone, U.S.A) and fetal bovine serum (FBS, Hyclone, USA) were purchased from Biodee Co., Ltd. Beijing. All other supplements/chemicals were from Sigma Aldrich and Alfa Aesar. Trimalonic acid modified C_{60} was synthesized according to the literature.[38]

The molecular weight of HSA, Gd-DTPA-HSA, and Gd-DTPA-HSA-C_{60} were measured by matrix assisted laser desorption/ionization time-of-flight mass spectrometry (MALDI-TOF-MS, AXIMA Shimadzu) with sinapic acid (SA) as the matrix. The Ultraviolet−visible (UV−vis) absorption features were taken by UV−vis spectroscopy (UV-4802H, UNIC). The Gd^{3+} concentrations were measured by inductively coupled plasma atomic emission spectroscopy (ICP-AES, ICPE-9000 Shimadzu). The cell internalization of macromolecular MRI contrast agents was confirmed by H-7650 transmission electron microscopy (TEM, Hitachi Ltd. Co, Japan).

The relaxation times were measured at three different magnetic fields: 0.5 T with NMI20 Analyst (Shanghai Niumag Corporation, Shanghai, China), 1.5 T Siemens Magnetom Sonata MRI Scanner (Siemens AG Erlangen, Germany) and 3 T clinical MR systems (Magnetom Trio, Siemens Medical Solutions, Erlangen, Germany). The inversion−recovery method was introduced to measure T_1 of the samples (300 μL) with different concentrations. The relaxivities r_1 in pure water and in saline were obtained from the slopes of the relaxation time (T_1) vs the Gd^{3+} concentration, respectively. T_1-weighted images at different concentrations in pure water and in saline were acquired on 1.5 and 3 T clinical MRI scanners, respectively. The parameters were T_R = 500 ms, T_E = 8 ms for 1.5 T and 8.9 ms for 3.0 T, slice thickness 2.0 mm, flip angle 90°, matrix 256 × 180, FOV 200 × 150, and for 0.5 T NMI20 analyst, using a spin−echo pulse sequence with pulse repetition time D_0 = 300 ms.

Preparation of Gd-DTPA-HSA Conjugate. A protocol for the direct reaction of DTPA-dianhydride with HSA and subsequent labeling with Gd^{3+} was applied. Briefly, 50 mg of HSA was dissolved in 5 mL of PBS (pH 7.4, 0.01 M); 50 mg of DTPA anhydride powder (the mole ratio of HSA:DTPA = 1:200) was added into the above solution directly and NaOH solution (0.1 M) was used to maintain the pH at 7.0. The resulting reaction mixture was stirred at 4 °C for 2 h. Afterward, the reaction solution was purified using the Sephadex G-25 with 0.5 M of HAc/NaAc buffer (pH 5.5) as elution. The content of HSA was evaluated by UV−vis spectroscopy. Subsequently, 50 mg of $GdCl_3{\cdot}6H_2O$ in 10 mL of HAc/NaAc buffer (pH 5.5) was added in the above purified DTPA-HSA conjugate, which was stirred gently at room temperature for 4 h. The resulting solution was dialyzed to remove the small molecules. The concentrated Gd-DTPA-HSA was further purified by ultrafiltration (10 000 MWCO, Millipore Corporation) to remove the residue impurities, and finally went through a Chelex-100 column to remove the redundant Gd^{3+} weakly complexed with HSA. Arsenazo III is used as an indicator to make sure the absence of free Gd^{3+}. Finally, the pure Gd-DTPA-HSA powder was obtained by lyophilizing the above purified solution for the following study.

Preparation of Gd-DTPA-HSA-C_{60} Conjugate. The trimalonic acid modified C_{60} was synthesized from the traditional Bingel-Hirsh reaction and then hydrolyzed by NaH to produce water-soluble fullerene derivatives.[38]

Briefly, 253 mg of C_{60} (0.35 mmol) and 200 μL of diethyl bromomalonate (1 mmol) were dissolved in 100 mL of toluene, then 173 μL of DBU (1,8-diazabicyclo[5,4,0]undec-7ene) (1 mmol) was dropped slowly into the above solution under argon atmosphere. The resulting solution was stirred continuously for 2 h at room temperature. The expected product (trimalonic ester modified C_{60}) in solution was separated by silica gel chromatography.

The obtained trimalonic ester modified C_{60} was dissolved in 50 mL of dried toluene and NaH (60% w/w suspension in mineral oil, 10 times excessive to the trimalonic ester modified C_{60}) was added in five batches. The resulting solution was stirred overnight under argon atmosphere at 70 °C. Afterward, 30 mL of MeOH was added and the solution was cooled to room temperature. Then, 10 mL of 25% HCl solution was added slowly to precipitate the product, which was further washed with Milli-Q water and dried under vacuum for 24 h to obtain the expected product $C_{60}[C(COOH)_2]_3$.

Ten milligrams of $C_{60}[C(COOH)_2]_3$ was dissolved in 5 mL of MES buffer solution (pH 6.0), 3-fold EDC/NHS was added into the above solution and stirred for 0.5 h at room temperature to give C_{60} carboxylate active ester intermediate. Afterward, 10 mg of Gd-DTPA-HSA was added and stirred for another 2 h to fulfill the conjugating reaction completely. Unreacted C_{60} derivatives were removed from the conjugates by the Millipore (10 000 MWCO) to give the desired product, Gd-DTPA-HSA-C_{60}. (Scheme 1)

DLS and Zeta Potential Measurement. Dynamic light scattering (DLS) measurements were performed on a commercial LS spectrometer (ALV/DLS/SLS-5022F) at 25 °C, which was equipped with a multi-τ digital time correlator (ALV5000) and a cylindrical 22 mW UNIPHASE He−Ne laser (λ = 632.8 nm). The scattering angle was fixed at 90°. Samples were filtered through a 0.22 μm pore size membrane before DLS measurement. The Zeta potentials were measured three times per sample by dynamic light scattering (NanoZS ZEN3600, Malvern) in Milli-Q water at pH about 6.8.

Transmetalation Stability Measurement. Briefly, 300 μL of as-prepared product in phosphate buffer (2.5 mM) was mixed with 10 μL of $ZnCl_2$ aqueous solution (2.5 mM), the resulting solution was surveyed by relaxation rate as a function of time for 2−4 days. The relative value of R_1 (t) at any time t, $R_1(t)/R_1(0)$, was evaluated as a good indicator of the extent of transmetalation.

Preparation of Sample for Cell TEM Characterization. Two hundred microliters of Gd-DTPA-HSA (0.5 mM) and 200 μL of Gd-DTPA-HSA-C_{60} (0.5 mM) were incubated with ca. 1 × 10^9 HeLa cell for 3 h, respectively. After complete lysis by trypsin, cells were washed by Hank's balanced salt solution (HBSS) to remove the non-internalized samples and then fixed overnight in 4% glutaraldehyde or

Scheme 1. Schematic Synthesis of Gd-DTPA-HSA and Gd-DTPA-HSA-C_{60}

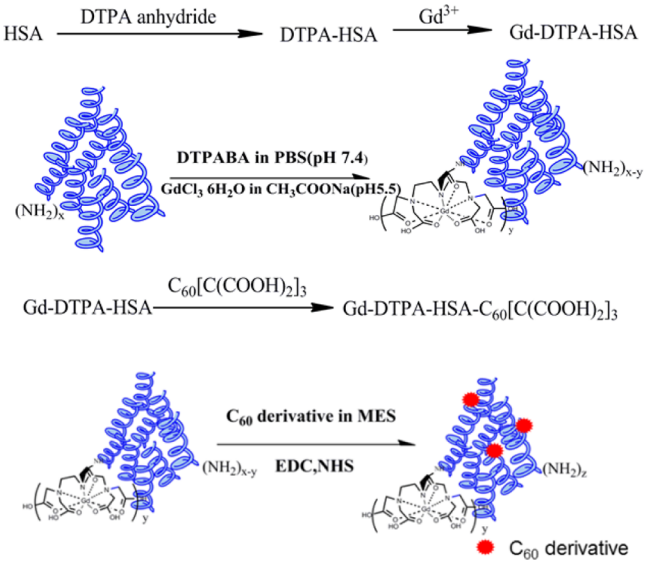

4% paraformaldehyde at 4 °C. Then cells were centrifugated under 1000 rpm for 5 min, and washed with 0.1 M of phosphate-buffered saline (PBS) for three times. All the cells were fixed in 3% glutaraldehyde containing blood plasma in small amount overnight at 4 °C for coagulating. Afterward the cells were postfixed with 1% osmium tetraoxide for 2 h at room temperature in 1 mm^3 masses. The cells were then dehydrated in a graded series of ethanol and acetone, and embedded in Epon812. Ultrathin section was cut by ultramicrotome (UC6, Leica Ltd. Co, Germany), and transferred onto 200-mesh copper grids, stained with uranyl acetate and lead nitrate and observed with a H-7650 TEM (Hitachi Ltd. Co, Japan).

In vitro Cellular MR Imaging. HeLa cells (10^6) were cultured in a culture dish, Gd-DTPA, Gd-DTPA-HSA or Gd-DTPA-HSA-C_{60} at the same gadolinium concentrations (0.03 mM) was added into the dish. After incubation for 8 h, the treated cells were washed with PBS for 3 times, and then suspended in PBS buffer to test MR imaging, untreated cells were used as a control. The T_1-weighted cellular MR imaging was taken at 0.5 T, 37 °C, using a spin−echo pulse sequence with pulse repetition time D_0 = 500 ms.

RESULT AND DISCUSSION

Structural Characterization. MALDI-TOF-MS results reveal that the molecular weight of Gd-DTPA-HSA-C_{60} locates at ca. 73,048 Da, which is ca. 7,076 Da larger than that of Gd-DTPA-HSA (65,972 Da), indicating that C_{60} derivatives (1026 Da) have been successfully modified on Gd-DTPA-HSA and the stoichiometry for Gd-DTPA-HSA: $C_{60}[C(COOH)_2]_3$ can be estimated as ca. 1:7 (see Figure S1 in the Supporting Information). Through Braford protein assay (see Figure S2 in the Supporting Information) and ICP-AES study, about 18 Gd-DTPA molecules were pay-loaded on each HSA.

For unraveling the size distribution of as-synthesized Gd-DTPA-HSA-C_{60} as well as Gd-DTPA-HSA, DLS measurements were performed. Figure 1 exhibits the hydrodynamic radius distributions of as-synthesized Gd-DTPA-HSA and Gd-DTPA-HSA-C_{60} in aqueous solution. Both Gd-DTPA-HSA and Gd-DTPA-HSA-C_{60} span a relatively wide size distribution and possess bimodal features, which is consistent with that of pristine HSA in water and saline (see Figure S3 in the Supporting Information). The peak values of Gd-DTPA-HSA in water and saline are 75 and 100 nm, respectively (Figure 1a), whereas those of Gd-DTPA-HSA-C_{60} show a relatively smaller

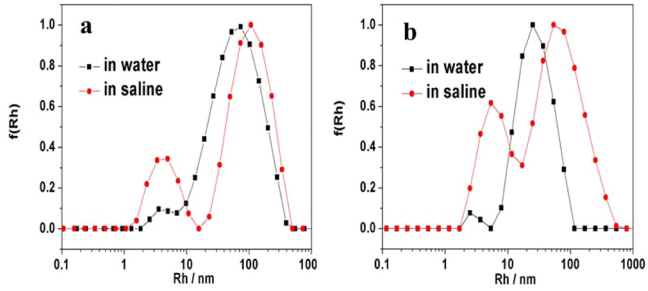

Figure 1. Hydrodynamic radius distributions of (a) Gd-DTPA-HSA and (b) Gd-DTPA-HSA-C_{60} in water and saline, respectively, measured by DLS.

sizes of ca.15 and 50 nm correspondingly (Figure 1b). The size decrease of Gd-DTPA-HSA-C_{60} aggregates relative to those Gd-DTPA-HSA may ascribe to the structural change of HSA induced by fullerene derivative, which has been revealed to effectively change the percentage of the HSA α-helix and β-sheet structure.[39] The size increase of Gd-DTPA-HSA-C_{60} (ca. 50 nm) and Gd-DTPA-HSA (ca. 100 nm) aggregates in saline relative to those in water may benefit from the protein salting out effect in saline as a result of increase between intermolecular interactions. In addition, the Zeta potentials of Gd-DTPA-HSA and Gd-DTPA-HSA-C_{60} were measured in Milli-Q water (pH 6.8) and saline (pH 7), respectively. As shown in Table 1, the increased Zeta potential of Gd-DTPA-

Table 1. Intensity Peak Values of Size Distribution Measured by DLS and Zeta Potentials for Gd-DTPA-HSA and Gd-DTPA-HSA-C_{60} in Water and Saline

compoundds	hydrodynamic radius (nm)	zeta potential (mV)
Gd-DTPA-HSA (in water)	75	−17.3
Gd-DTPA-HSA (in saline)	100	−11.8
Gd-DTPA-HSA-C_{60} (in water)	15	−24.6
Gd-DTPA-HSA-C_{60} (in saline)	50	−11.0

HSA-C_{60} in water (−24.6 mV) relative to that of Gd-DTPA-HSA (−17.3 mV) should favor the resulting stable, relatively small and well dispersible aggregates. Notably, the Zeta potentials of Gd-DTPA-HSA-C_{60} and Gd-DTPA-HSA in saline dramatically decrease to −11.0 and −11.8 mV, respectively, because of the salting out effect induced structural change of macromolecular Gd-complex, which may contribute a little to the size increase of the obtained aggregates.

In vitro MRI Study. To evaluate the contrast enhancement of obtained macromolecular Gd-complex, we measured the relaxivity r_1 at three different magnetic fields, 3, 1.5, and 0.5 T, using commercial $[Gd\text{-}DTPA\ (H_2O)]^{2-}$ (Magnevist) and its precursor Gd-DTPA-HSA as control. From the results shown in Table 2, we can see clearly that the relaxivities of macromolecular Gd-complex, Gd-DTPA-HSA and Gd-DTPA-HSA-C_{60}, are field strength dependent and increase with the decrease of field strength in both water and saline, for example, 19.4/25.0 mM^{-1} s^{-1} at 3 T, 26.4/38.0 mM^{-1} s^{-1} at 1.5 T (see Figures S4 and S5 in the Supporting Information), and 37.8/86.0 mM^{-1} s^{-1} at 0.5 T (Figure 3a, b) in water, for Gd-DTPA-HSA/Gd-DTPA-HSA-C_{60}, respectively. In contrast, the relaxivities of small molecular MRI contrast agent, $[Gd\text{-}DTPA\ (H_2O)]^{2-}$(Magnevist), are almost constant (3.9, 4.7, and 4.5 mM^{-1} s^{-1} at 3, 1.5, and 0.5 T, respectively) at different

dx.doi.org/10.1021/am300817z | ACS Appl. Mater. Interfaces 2012, 4, 3724−3729

Table 2. Comparison of Relaxivities (in units of $mM^{-1}s^{-1}$ per mM of gadolinium ion)

compounds	relaxivity r_1 (mM^{-1} s^{-1}) (at 300 K)		
	3 T	1.5 T	0.5 T
Gd-DTPA	3.9	4.7	4.5
Gd-DTPA-HSA (in water)	19.4	26.4	37.8
Gd-DTPA-HSA (in saline)	14.4	23.5	31.5 (310 K)
Gd-DTPA-HSA-C_{60} (in water)	25.0	38.0	86.0
Gd-DTPA-HSA-C_{60} (in saline)	19.0	32.9	58.4 (310 K)

field strengths, which is well-consistent with the literature.[20] Notably, although the hydrodynamic radius of formed aggregates increases in saline (100 nm vs 75 nm for Gd-DTPA-HSA and 50 nm vs 15 nm for Gd-DTPA-HSA-C_{60} in saline and water, respectively), the relaxivities of macromolecular Gd-complex under this condition slightly decrease relative to those in water at the same field strength, such as 31.5 mM^{-1} s^{-1} vs 37.8 mM^{-1} s^{-1} for Gd-DTPA-HSA and 58.4 mM^{-1} s^{-1} vs 86.0 mM^{-1} s^{-1} for Gd-DTPA-HSA-C_{60} at 0.5 T. This result is much different from those gadofullerene MRI contrast agents since the relaxivities of latter dramatically decrease in saline due to the disaggregation of nanoparticles.[40] This abnormal phenomenon should ascribe to the salting out effect, which can induce structural reconstruction of Gd-DTPA-HSA and Gd-DTPA-HSA-C_{60} and reduce the restraint to payloaded Gd-DTPA and thus weaken the effect of macromolecule on rotational correlation time of Gd-DTPA. The T_1-weight imaging in vitro displayed in Figures 2 and 3c was well in agreement with the relaxivity results.

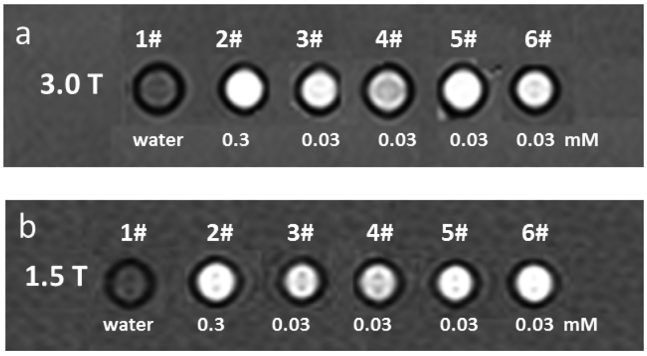

Figure 2. T_1-weighted images with D_0 = 500 ms, at (a) 3.0 T and (b) 1.5 T at 298 K. From 1# to 6#: water (1#), Gd-DTPA (2#), Gd-DTPA-HSA in water (3#), Gd-DTPA-HSA in saline (4#); Gd-DTPA-HSA-C_{60} in water (5#), and Gd-DTPA-HSA-C_{60} in saline (6#).

As we know, the rotational correlation time τ_R as one of the pivotal parameters that determine the relaxivity, is defined by eq 1, in which a, η, k, and T represent the radius, the viscosity of agent, Boltzmann constant, and Kelvin temperature, respectively.

$$\tau_R = 4\pi a^3 \eta / 3kT \quad (1)$$

From the equation, we know that the size of molecule is closely related with τ_R. Herein, when small molecular Gd-DTPA is attached to HSA, the size of the conjugate Gd-DTPA-HSA increases compared to Gd-DTPA, leading to the decrease of rotation of the whole molecule, and as a consequence, the relaxivity increases. Proton relaxation will be optimum when the fluctuating magnetic field is in resonance close to the

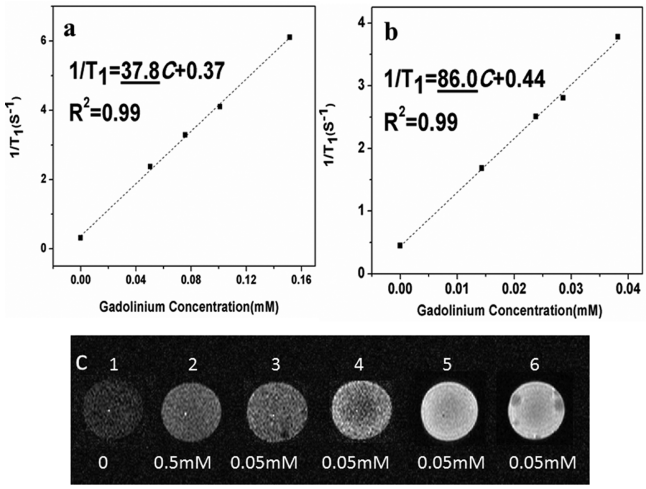

Figure 3. Linear relationship between T_1 relaxation rates ($1/T_1$) and Gd^{3+} ion concentrations for (a) Gd-DTPA-HSA, (b) Gd-DTPA-HSA-C_{60} in water at 0.5 T and 300 K, and (c) T_1-weighted images with D_0 = 300 ms, at 0.5 T and 310 K. From 1# to 6#: water (1#), Gd-DTPA (2#), Gd-DTPA-HSA in water (3#), Gd-DTPA-HSA in saline (4#); Gd-DTPA-HSA-C_{60} in water (5#), and Gd-DTPA-HSA-C_{60} in saline (6#).

proton Larmor frequency. Through ^{1}H-NMRD studying of the proton relaxivity at different magnetic field, the maximum mainly appears at ca. 20 MHz. Brasch has studied the relaxivity of Albumin-Gd-DTPA conjugate and the measured relaxivity is 20 mM^{-1} s^{-1} at 10 MHz.[41] MS-325 is a blood-pool CA, which could noncovalently bind to albumin, exhibiting a relaxivity of 40−50 mM^{-1} s^{-1} at 20 MHz.[19] In this work, the covalent interaction between HSA and Gd-DTPA leads to relaxivity of 37.8 mM^{-1} s^{-1} at 20 MHz, which is comparable to the literature. However, once the Gd-DTPA-HSA complex was further conjugated with fullerene derivatives to give Gd-DTPA-HSA-C_{60} (18:1:7), the resulting relaxivity dramatically increases to 86.0 mM^{-1} s^{-1} at 0.5 T, comparable to the predicted by theory (80−120 mM^{-1} s^{-1}, under the same condition). This phenomenon may ascribe to the novel fullerene induced reconstruction of macromolecular structure, leading to an optimized self-assembling, and the resulting aggregate possesses Larmor procession frequency in close proximity to the low magnetic field strength. In addition, the involved fullerene is also an effective photosensitizer suitable for PDT[35,42] and thus endows the assembling complex with the modalities of therapy (PDT) and diagnostic imaging (MRI).

Transmetalation Stability. Different from the small molecular MRI contrast agents, macromolecular conjugates favor longer resident lifetime in the body and incomplete elimination, which increase the risk of potential release of toxic free gadolinium(III) and ligands. The transmetalation experiments were therefore explored according to the Muller's method[43] to investigate the stability of Gd-DTPA-HSA and Gd-DTPA-HSA-C_{60}. The results revealed that the stability of Gd-DTPA-HSA-C_{60} negligibly decreases relative to that of its precursor Gd-DTPA-HSA (Figure 4), both of which are stable enough for further in vivo study.[44]

Transmission Electron Microscopy. To make sure there is the possibility of cellular uptake for the obtained macromolecular conjugates, cell TEM is performed as below. The results shown in Figure 5 confirm unambiguously that both Gd-DTPA-HSA and Gd-DTPA-HSA-C_{60} can be internalized into

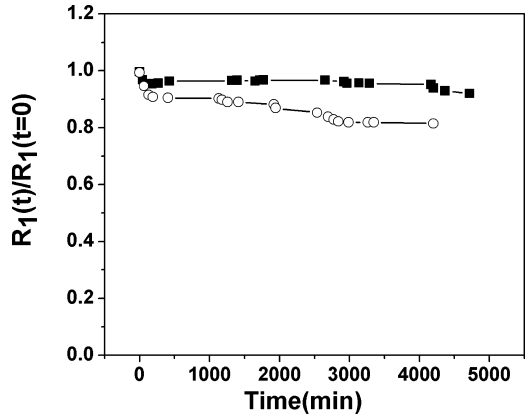

Figure 4. Evolution $R_1(t)/R_1(t = 0)$ as a function of time for Gd-DTPA-HSA (■) and Gd-DTPA-HSA-C_{60} (○).

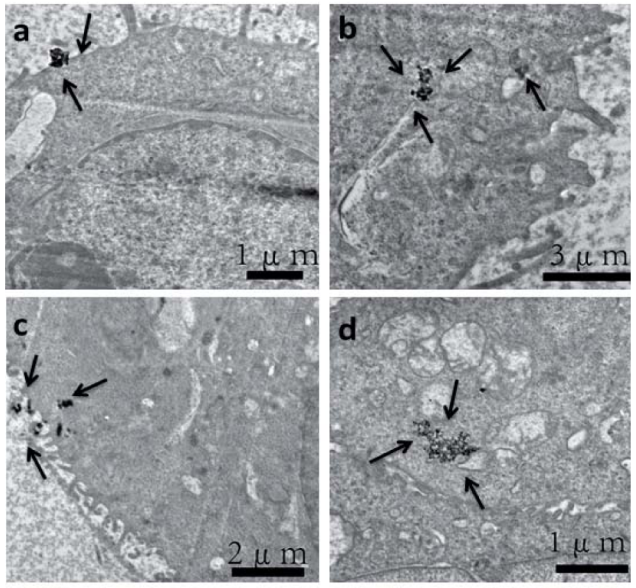

Figure 5. Transmission electron microscopy images of (a) Gd-DTPA-HSA internalized into cell via transmembrane, (b) Gd-DTPA-HSA located in the cytoplasm and autophagosome, (c) Gd-DTPA-HSA-C_{60} internalized into cells through endocytosis, and (d) Gd-DTPA-HSA-C_{60} located within the cytoplasm.

HeLa cells (Figure 5b,d) via trans-membrane (Figure 5a) or through endocytosis (Figure 5c), indicating the great potential of this kind of molecular MRI contrast agent to report molecular events at the cellular and subcellular levels. Importantly, the highly efficient macromolecular MRI contrast agent once is targeting modified and pay-loaded with drug,[45] it will make theranostic function integrative.

In vitro Cellular MR Imaging. To further evaluate the macromolecular contrast agents at the cellular level, MR imaging experiments were performed on HeLa cells incubated with Gd-DTPA-HSA or Gd-DTPA-HSA-C_{60}, Gd-DTPA and untreated cells were used as control. As Figure 6 reveals that the sequence for contrast enhancement is Gd-DTPA-HSA-C_{60} > Gd-DTPA-HSA ≫ Gd-DTPA > control at the same gadolinium concentration (0.03 mM), suggesting that the two kinds of macromolecular contrast agents could be used as the potential MRI CAs to sensitively image the events at the cellular and subcellular levels.

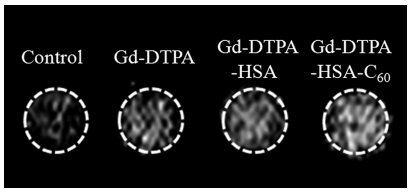

Figure 6. Cellular MR imaging at gadolinium concentration of 0.03 mM, 0.5 T, and D_0 = 500 ms.

CONCLUSION

We have successfully used Gd-DTPA-HSA as a model to conjugate with fullerene derivative to obtain a highly efficient MRI contrast agent, Gd-DTPA-HSA-C_{60}. The optimized structure of conjugates leads to the relaxivity as high as 86 mM^{-1} s^{-1} at 0.5 T and 300 K, which is the maximal reported so far and comparable to the theoretical maximum (r_1 = 80−120 mM^{-1} s^{-1}, at 20 MHz and 298 K). The effectively cellular uptake indicates its potential application in report of the events at the cellular and subcellular levels. Because the incorporation of fullerene in Gd-DTPA-HSA will further endow the resulting complex with PDT property, the highly efficient MRI contrast agent may simultaneously address the optimized therapeutical time range of this hybrid system for tumor treatment. The investigation of in vivo distribution and pharmacokinetics behavior is ongoing.

ASSOCIATED CONTENT

Supporting Information

Experimental details; MALDI-TOF-MS of HSA, Gd-DTPA-HSA, and Gd-DTPA-HSA-C_{60}[$C(COOH)_2]_3$; the work curve of Coomassie brilliant blue, the DLS data of HSA, the linear relationship between T_1 relaxation rates ($1/T_1$) and Gd^{3+} ion concentrations for Gd-DTPA-HSA and Gd-DTPA-HSA-C_{60} in water and in saline at 3 and 1.5 T clinic magnetic fields, respectively. This material is available free of charge via the Internet at http://pubs.acs.org/.

AUTHOR INFORMATION

Corresponding Author

*E-mail: shucy@iccas.ac.cn (C.S.); crwang@iccas.ac.cn (C.W.).

Notes

The authors declare no competing financial interest.

ACKNOWLEDGMENTS

This work is supported by 973 Program (2011CB302100), the National Natural Science Foundation of China (21121063, 51072200, 31170963), NSAF (11076027), and the Project-sponsored by SRF for ROCS, SEM.

REFERENCES

(1) Sosnovik, D. E.; Weissleder, R. *Curr. Opin. Biotechnol.* **2007**, *18*, 4−10.
(2) Caravan, P.; Ellison, J. J.; McMurry, T. J.; Lauffer, R. B. *Chem. Rev.* **1999**, *99* (9), 2293−2352.
(3) Terreno, E.; Castelli, D. D.; Viale, A.; Aime, S. *Chem. Rev.* **2010**, *110* (5), 3019−3042.
(4) Weissleder, R. *Science* **2006**, *312*, 1168−1171.
(5) Liu, G. Z.; Charlotte, E. C.; Drummond, C. J. *J. Phys. Chem. B* **2009**, *113*, 15949−15959.
(6) Cheng, Z. L.; Thorek, D. L. J.; Tsourkas, A. *Adv. Funct. Mater.* **2009**, *19* (23), 3753−3759.

(7) Villaraza, A. J. L.; Bumb, A.; Brechbiel, M. W. *Chem. Rev.* **2010**, *110* (5), 2921−2959.
(8) Shu, C. Y.; Corwin, F. D.; Zhang, J. F.; Chen, Z. J.; Reid, J. E.; Sun, M. H.; Xu, W.; Sim, J. H.; Wang, C. R.; Fatouros, P. P.; Esker, A. R.; Gibson, H. W.; Dorn, H. C. *Bioconjugate Chem.* **2009**, *20*, 1186−1193.
(9) Yoon, S. Y.; Lee, B.; Lee, K. S.; Im, G. H.; Byeon, S. H.; Lee, J. H.; Lee, I. S. *Adv. Funct. Mater.* **2009**, *19*, 3375−3380.
(10) Manus, L. M.; Mastarone, D. J.; Waters, E. A.; Zhang, X. Q.; Schultz-Sikma, E. A.; Macrenaris, K. W.; Ho, D.; Meade, T. J. *Nano Lett.* **2010**, *10* (2), 484−489.
(11) Kobayashi, H.; Kawamoto, S.; Jo, S. K.; Bryant, H. L.; Brechbiel, M. W.; Star, R. A. *Bioconjugate Chem.* **2003**, *14* (2), 388−394.
(12) Sitharaman, B.; Kissell, K. R.; Hartman, K. B.; Tran, L. A.; Baikalov, A.; Rusakova, I.; Sun, Y.; Khant, H. A.; Ludtke, S. J.; Chiu, W.; Laus, S.; Tóth, E.; Helm, L.; Merbach, A. E.; Wilson, L. J. *Chem. Commun.* **2005**, *31*, 3915−3917.
(13) Xu, Z. P.; Kurniawan, N. D.; Bartlett, P. F.; Lu, G. Q. *Chem.—Eur. J.* **2007**, *13* (10), 2824−30.
(14) Laus, S.; Ruloff, R. *Chem.—Eur. J.* **2003**, *9*, 3555−3566.
(15) Doble, D. M.; Botta, M.; Wang, J.; Aime, S.; Barge, A.; Raymond, K. N. *J. Am. Chem. Soc.* **2001**, *123* (43), 10758−10759.
(16) Yang, J. J.; Yang, J.; Wei, L.; Zurkiya, O.; Yang, W.; Li, S.; Zou, J.; Zhou, Y.; Maniccia, A. L. W.; Mao, H.; Zhao, F.; Malchow, R.; Zhao, S.; Johnson, J.; Hu, X.; Krogstad, E.; Liu, Z. R. *J. Am. Chem. Soc.* **2008**, *130* (29), 9260−9267.
(17) Ananta, J. S.; Godin, B.; Sethi, R.; Moriggi, L.; Liu, X. W.; Serda, R. E.; Krishnamurthy, R.; Muthupillai, R.; Bolskar, R. D.; Helm, L.; Ferrari, M.; Wilson, L. J.; Decuzz, P. *Nat Nanotechnol.* **2010**, *5*, 815−821.
(18) Carney, C. E.; Tran, A. D.; Wang, J.; Schabel, M. C.; Sherry, A. D.; Woods, M. *Chem.—Eur. J.* **2011**, *17* (37), 10372−8.
(19) Caravan, P.; Cloutier, N. J.; Greenfield, M. T.; McDermid, S. A.; Dunham, S. U.; Bulte, J. W. M.; Amedio, J. C.; Looby, R. J.; Supkowski, R. M.; Horrocks, W. D.; McMurry, T. J.; Lauffer, R. B. *J. Am. Chem. Soc.* **2002**, *124* (12), 3152−3162.
(20) Frullano, L.; Wang, C.; Miller, R. H.; Wang, Y. *J. Am. Chem. Soc.* **2011**, *133*, 1611−1613.
(21) Laus, S.; Ruloff, R.; Tóth, E.; Merbach, A. E. *Chem.—Eur. J.* **2003**, *9* (15), 3555−66.
(22) Livramento, J. B.; Toth, E.; Sour, A.; Borel, A.; Merbach, A. E.; Ruloff, R. *Angew. Chem., Int. Ed.* **2005**, *44*, 1480−1484.
(23) Laus, S.; Sour, A.; Ruloff, R.; Tóth, É.; Merbach, A. E. *Chem.—Eur. J.* **2005**, *11*, 3064−3076.
(24) Raymond, K. N.; Pierre, V. C. *Bioconjugate Chem.* **2005**, *16*, 3−8.
(25) Werner, E. J.; Avedano, S.; Botta, M.; Hay, B. P.; Moore, E. G.; Aime, S.; Raymond, K. N. *J. Am. Chem. Soc.* **2007**, *129*, 1870−1871.
(26) Rudovsky, J.; Botta, M.; Hermann, P.; Hardcastle, K. I.; Lukes, I.; Aime, S. *Bioconjugate Chem.* **2006**, *17*, 975−987.
(27) Avedano, S.; Tei, L.; Lombardi, A.; Giovenzana, G. B.; Aime, S.; Longo, D.; Botta, M. *Chem. Commun.* **2007**, *45*, 4726−8.
(28) Benedict, L.; Hsuan, T. C. *Bioconjugate Chem.* **2009**, *20* (9), 1683−1695.
(29) Villaraza, A. J. L.; Bumb, A.; Brechbiel, M. W. *Chem. Rev.* **2010**, *110*, 2921−2959.
(30) Conyers, J. L. *Nanomedicine* **2009**, *4*, 261−275.
(31) Bakry, R.; Najam, M.; Huck, C. W. *Nanomedicine* **2007**, *2* (4), 639−649.
(32) Maeda, R.; Noiri, E.; Isobe, H.; Nakanishi, W.; Okamoto, K.; Doi, K.; Sugaya, T. *Proc. Natl. Acad .Sci.* **2010**, *107* (12), 5339−5344.
(33) Zakharian, T. Y.; Seryshev, A.; Sitharaman, B.; Gilbert, B. E.; Knight, V.; Wilson, L. J. *J. Am. Chem. Soc.* **2005**, *127*, 12508−12509.
(34) Liu, J.; Ohta, S. I.; Sonoda, A.; Yamada, M.; Yamamoto, M.; Norihisa, N.; Murata, K.; Tabata, Y. *J. Controlled Release* **2007**, *117*, 104−110.
(35) Partha, R.; Mitchell, L. R.; Lyon, J. L.; Joshi, P. P.; Conyers, J. L. *ACS Nano* **2008**, *2* (9), 1950−1958.
(36) Belgorodsky, B.; Fadeev, L.; Ittah, V.; Benyamini, H.; Zelner, S. *Bioconjugate Chem.* **2005**, *16*, 1058−1062.
(37) Qu, X.; Komatsu, T.; Sato, T.; Glatter, O.; Horinouchi, H.; Kobayashi, K. *Bioconjugate Chem.* **2008**, *19*, 1556−1560.
(38) Bingel, C. *Chem. Ber.* **1993**, *126* (8), 1957−1959.
(39) Zhang, X. F.; Shu, C. Y.; Xie, L.; Wang, C. R.; Zhang, Y. Z.; Xiang, J. F.; Li, L.; Tang, Y. L. *J. Phys. Chem. C* **2007**, *111*, 14327−14333.
(40) Laus, S.; Sitharaman, B.; Toth, V.; Bolskar, R. D.; Helm, L.; Asokan, S.; Wong, M. S.; Wilson, L. J.; Merbach, A. E. *J. Am. Chem. Soc.* **2005**, *127* (26), 9368−9369.
(41) Schmiedl, U. O.; Hannu, M. P.; Crooks, E.; Robert, B. C. *Radiology* **1987**, *162*, 205−210.
(42) Mroz, P.; Tegos, G. P.; Gali, H.; Wharton, T.; Sarna, T.; Hamblin, M. R. *Photochem. Photobiol. Sci.* **2007**, *6*, 1139−1149.
(43) Laurent, S. L.; Henoumont, C.; Muller, R. N. *Contrast Media Mol. Imaging* **2010**, *5* (6), 305−308.
(44) Kim, H. K.; Park, J. A.; Kim, K. M.; Md, N. S.; Kang, D. S.; Lee, J.; Chang, Y.; Kim, T. J. *Chem. Commun.* **2010**, *46*, 8442−8446.
(45) Temming, K.; Lacombe, M.; Hoeven, P.; Prakash, J.; Gonzalo, T. *Bioconjugate Chem.* **2006**, *17*, 1246−1255.